

Article

Microstructural Evolution and Tensile Testing of a Bi–Sn (57/43) Alloy Processed by Tube High-Pressure Shearing

Chuan-Ting Wang ¹, Zheng Li ², Yong He ^{1,*}, Jing-Tao Wang ² and Terence G. Langdon ^{3,4,*}

¹ School of Mechanical Engineering, Nanjing University of Science & Technology, Nanjing 210094, China; ctwang@njjust.edu.cn

² School of Materials Science and Engineering, Nanjing University of Science & Technology, Nanjing 210094, China; lizheng@njjust.edu.cn (Z.L.); jtwang@njjust.edu.cn (J.-T.W.)

³ Departments of Aerospace & Mechanical Engineering and Materials Science, University of Southern California, Los Angeles, CA 90089-1453, USA

⁴ Materials Research Group, Department of Mechanical Engineering, University of Southampton, Southampton SO17 1BJ, UK

* Correspondence: yonghe1964@163.com (Y.H.); langdon@usc.edu (T.G.L.)

Abstract: Tube high-pressure shearing (t-HPS) processing was performed on a eutectic Bi–Sn (57/43) alloy for 0.25, 1, 5 and 20 turns. The selected samples were stored at room temperature for up to 56 days to examine the strain weakening and self-annealing behavior of the alloy. The results showed that t-HPS processing gradually refined the microstructure and led to decreasing of microhardness, but microhardness increased slowly during the subsequent storage at room temperature. Shear localization of the eutectic structure during t-HPS processing was observed as large amounts of narrow dense lamellar zones were visible in the deformed microstructures. The Bi–Sn (57/43) alloy processed by t-HPS exhibited significantly enhanced superplastic properties with elongations up to >1800% in a sample after t-HPS processing for 20 turns. This high elongation is attributed to the breaking of the lamellar structure and the very small grain size.

Keywords: Bi–Sn alloy; microhardness; self-annealing; superplasticity; tube high-pressure shearing



Citation: Wang, C.-T.; Li, Z.; He, Y.; Wang, J.-T.; Langdon, T.G.

Microstructural Evolution and Tensile Testing of a Bi–Sn (57/43) Alloy Processed by Tube High-Pressure Shearing. *Crystals* **2021**, *11*, 1229.

<https://doi.org/10.3390/cryst11101229>

Academic Editor: Wojciech Polkowski

Received: 30 September 2021

Accepted: 9 October 2021

Published: 12 October 2021

Publisher's Note: MDPI stays neutral with regard to jurisdictional claims in published maps and institutional affiliations.



Copyright: © 2021 by the authors. Licensee MDPI, Basel, Switzerland. This article is an open access article distributed under the terms and conditions of the Creative Commons Attribution (CC BY) license (<https://creativecommons.org/licenses/by/4.0/>).

1. Introduction

Considerable interest has developed over the last two decades to producing and measuring the mechanical properties of materials with exceptionally small grain sizes. Ultrafine-grained (UFG) metals are defined specifically as metals where the average grain size is less than $\sim 1 \mu\text{m}$ [1] and these small grains divide into the two categories of sub-micrometer grains with sizes of 100–1000 nm and nanometer grains where the average size is $< 100 \text{ nm}$. An advantage in producing these materials is that they exhibit high strength and there is a potential for achieving superplastic elongations at exceptionally rapid strain rates which would be advantageous for manufacturing parts in the superplastic forming industry [2]. Materials with UFG structures are generally produced using procedures based on the application of severe plastic deformation (SPD) where the material is subjected to a very high strain but without any significant changes in the overall dimensions of the workpiece. As discussed in a comprehensive review [3], the two main techniques of SPD processing are equal channel angular pressing (ECAP), where a rod or a bar is pressed through a die constrained within a channel bent through a sharp angle [4], and high-pressure torsion (HPT), where the sample is generally in the form of a thin disk subjected to high pressure and concurrent torsional straining [5].

Both ECAP and HPT are effective for processing to produce metals with very small grains, but the procedures are different because ECAP is a discontinuous and labor-intensive process in which the sample is removed and then reinserted into the die between each pass whereas HPT is a continuous process where the sample is torsionally strained up

to the required maximum numbers of rotations. In practice, the experiments show that processing by HPT has two advantages over ECAP because it produces smaller grain sizes [6,7] and a larger fraction of grain boundaries with large angles of misorientation [8–12]. Nevertheless, HPT processing has a significant disadvantage because the processed samples are generally very small and therefore they can be used in small-scale applications such as electronic devices but cannot be utilized in large-scale industrial applications.

To overcome this deficiency while at the same time using a processing method based on the application of shearing, an alternative approach was developed which is known as tube high-pressure shearing (t-HPS). This is a new and novel SPD technique that was used effectively to process commercial purity aluminum [13] and also to produce a multilayered structure using pure Pb and pure Sn as prototype materials [14,15].

To date, very few results are available on the processing of materials by t-HPS although the procedure appears promising for fabricating UFG metals. Accordingly, the objective of this study was to examine the microstructural evolution associated with t-HPS, consider the effect of the occurrence of self-annealing after the processing operation and conduct tensile testing to evaluate the potential for achieving good superplastic properties. The experiments were conducted using the Bi–Sn eutectic alloy where this material was chosen for two reasons. First, a very recent study using HPT showed that this alloy exhibited extensive self-annealing but with good superplastic behavior [16,17]. Second, a very early investigation representing the first report of true superplasticity in any metal showed that the Bi–Sn eutectic alloy in an extruded condition exhibited exceptionally high elongations to failure in tensile testing [18].

2. Experimental Material and Procedures

Tubular samples of the Bi–Sn (57/43 wt%) eutectic alloy were cast from a mixture of Bi and Sn beads with purities of 99.99%. The principle of the t-HPS process was introduced earlier [13] and basically the procedure in t-HPS is that a tubular sample with an outer radius of around 47.7 mm and a wall thickness of around 2.7 mm is placed in the gap between the central mandrel and the outer cylinder of the t-HPS facility and high hydrostatic pressure is introduced to the sample by compressing the pressure rings placed at the upper and lower ends of the tubular sample. As the outer cylinder rotates, the large frictional force at the interfaces between the central mandrel/outer cylinder and the sample drags the sample to shear. The rotation speed in these experiments was set to about 0.2 turns per minute. The samples were processed by t-HPS through a total number (n) of 1/4, 1, 5 and 20 turns. Following t-HPS, self-annealing was conducted by storing the samples at room temperature (RT) for various times up to a maximum of 56 days.

The samples were etched using a solution of FeCl_3 after polishing. X-ray diffraction (XRD) (Cu K α radiation) was employed to examine the Bi–Sn samples after processing with the diffractometer set to around 0.015° per step. The microstructures of the selected samples were observed with a scanning electron microscope (SEM) JEOL JSM-7001 operating at a voltage of 15 kV. Microhardness values were recorded using a Vickers hardness tester with a load of 50 gf and dwell times of 10 s. Focused ion beam (FIB) was employed to investigate the nature of the Sn particles within the Bi phase after HPT processing and storage at RT. The ion beam voltage of the FIB was 30 kV and the final milling current was 50 pA. The cross-section of the disk sample was milled so that the Sn particles became visible.

After t-HPS processing, the tube samples were firstly flattened slowly to form a long sample. Then, tensile samples with gauge lengths of 3 mm and widths of 2 mm were machined from the long samples. The thickness of these samples was around 2 mm. Tensile tests were performed on these samples using an Instron testing facility under initial strain rates of 1.0×10^{-2} , 1.0×10^{-3} and $1.0 \times 10^{-4} \text{ s}^{-1}$ at room temperature.

3. Experimental Results

Figure 1 shows the microstructures of the Bi–Sn alloy (a) in the as-cast condition and after t-HPS processing for (b) 0.25, (c) 1, (d) 5 and (e) 20 turns, where the SEM observations

were conducted after storage at RT for 8 h following t-HPS processing. Inspection showed the as-cast Bi–Sn alloy has a typical eutectic structure where the Bi phase and the Sn phase are complementary and packed together. As the etchant preferentially attacked the Sn phase, large amounts of very small Bi precipitate particles became visible within the Sn-rich areas after etching. After t-HPS processing for 0.25 and 1 turn, no significant microstructural change was observed despite some slight rotation of the lamellar structure, and the overall eutectic structure was not destroyed. As the number of turns increased to 5 and 20, it was observed that each phase started to fracture. The edges of both phases became sharper and grains with equiaxed shapes became visible.

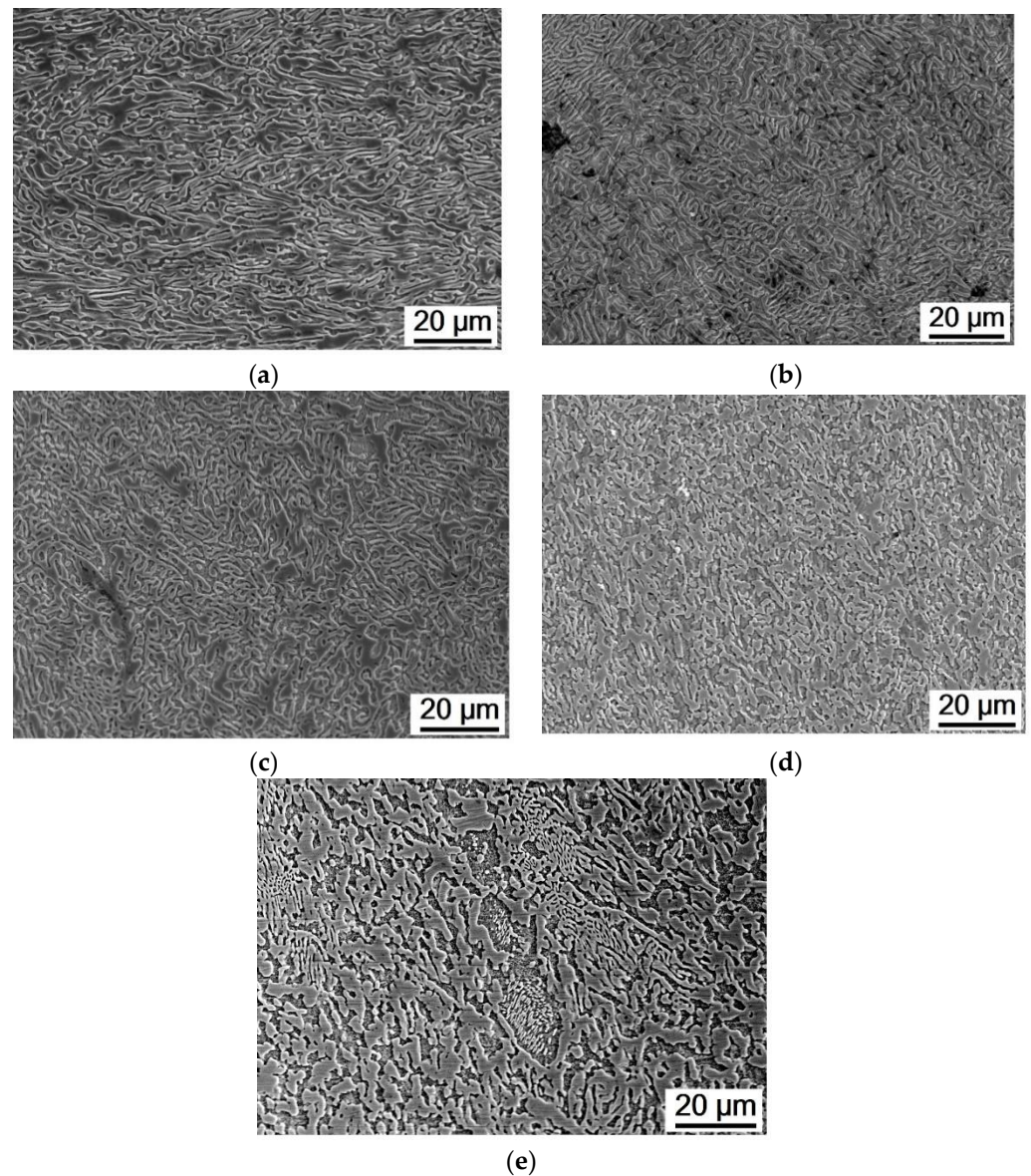


Figure 1. Microstructure of the Bi–Sn samples in (a) the as-cast condition and after t-HPS processing for (b) 0.25, (c) 1, (d) 5 and (e) 20 turns and storage at RT for 8 h.

The XRD spectra of a Bi–Sn sample in the as-cast condition and after t-HPS processing for five turns are shown in Figure 2 where the peaks of pure Bi and Sn are indicated. The XRD pattern reveals that the Bi–Sn (57/43) alloy is composed of pure Bi and pure Sn elements only and no binary compound is detected.

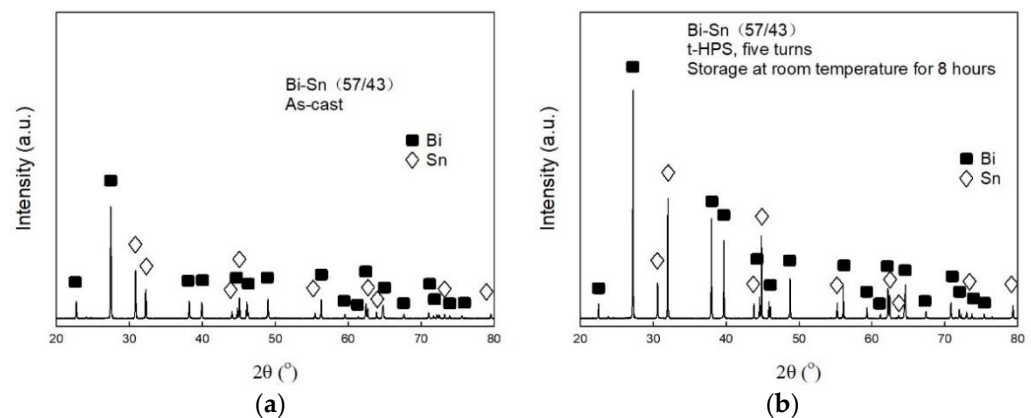


Figure 2. XRD spectrum of the Bi–Sn samples in (a) the as-cast condition and (b) after t-HPS processing for five turns and storage at RT for 8 h.

When the microstructure was observed under a lower magnification, it was noticed that the shear deformation was not homogeneous and there were some narrow dense lamellar bands visible in the matrix. As shown in Figure 3a, the width of these bands was around 10–20 μm after five turns of t-HPS processing. The phase inside such bands preserved the original lamellar structure of the as-cast sample while the phase structure outside these bands consisted of equiaxed grains. After 20 turns of deformation, the length of dense lamellar bands was much shorter.

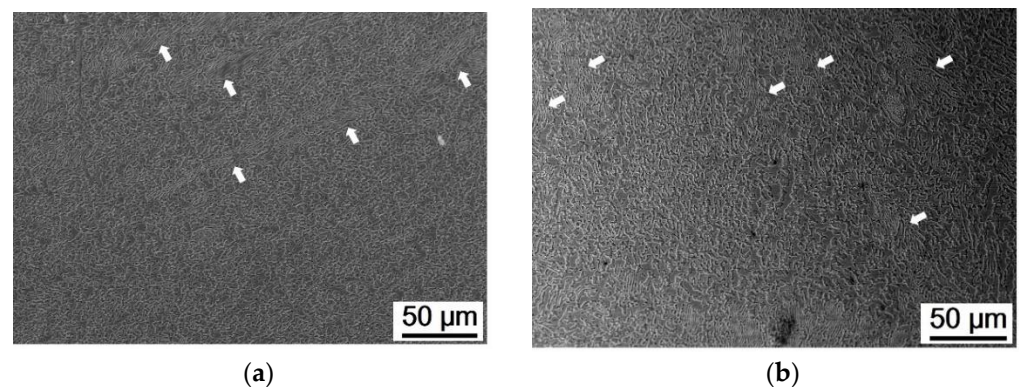


Figure 3. Microstructure of the Bi–Sn samples after t-HPS processing for (a) 5 and (b) 20 turns and storage at RT for 8 h, with arrows indicating the lamellar bands.

A Bi–Sn sample processed by t-HPS for five turns was used to evaluate the evolution of microhardness during storage at RT. Microhardness indentations were recorded for the sample and these measured values were then plotted against the number of days of storage as shown in Figure 4. The as-cast Bi–Sn (57/43) alloy had microhardness of $\sim 22.5 \pm 0.5$ Hv. The microhardness values were recorded as $\sim 11.1 \pm 0.9$ Hv after t-HPS processing and storage for 8 h at RT. Microhardness increased gradually during storage, reaching $\sim 13.0 \pm 0.5$ Hv after 7 days of storage, and further increased to $\sim 14.4 \pm 0.3$ Hv and $\sim 14.9 \pm 0.7$ Hv after 42 days and 56 days of storage, respectively. Similar behavior was widely reported in low melting temperature materials processed by severe plastic deformation, for example, in the Zn–Al, Sn–Pb and Bi–Sn alloys [16,17,19–22]. However, it is worth noting that microhardness of the Bi–Sn (57/43) alloy after t-HPS processing is more stable compared to the condition after processing by HPT. As shown in an earlier study, microhardness of the Bi–Sn alloy dropped from ~ 25.2 Hv to around 8 Hv after processing by HPT for five turns, and thereafter microhardness increased to around 17 Hv after 7 days of storage at room temperature [16,17].

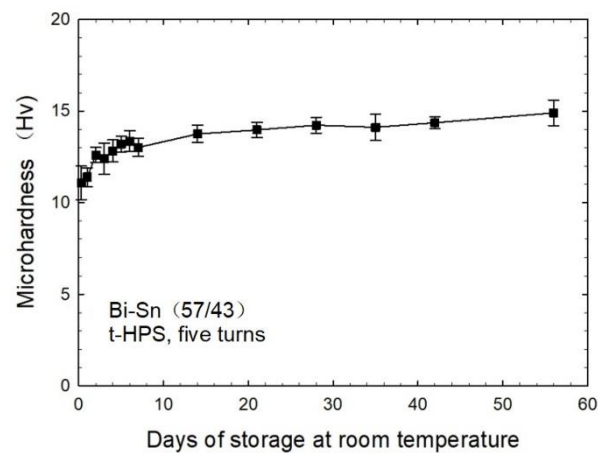


Figure 4. Microhardness of the Bi–Sn samples versus the number of days of storage at RT after t-HPS processing for five turns.

Figure 5 shows the microstructures of the Bi–Sn samples after storage at RT for various periods. The Sn phase was etched away by the etchant so that the Bi phase is clearly visible in the images. As shown in Figure 5a, the phase structure was broken by the shear stain and there were large numbers of Bi phase islands with essentially equiaxed shape. As the number of storage days increased, the Bi phase grew and connected together again so that the total number of small Bi islands decreased. Moreover, it is observed in all of these images that pitting holes existed inside the Bi phase where these pitting holes had sizes of around several hundred nanometers. It is reasonable to expect that these pitting holes were pre-resolved Sn particles within the Bi phase which were etched away by the etchant.

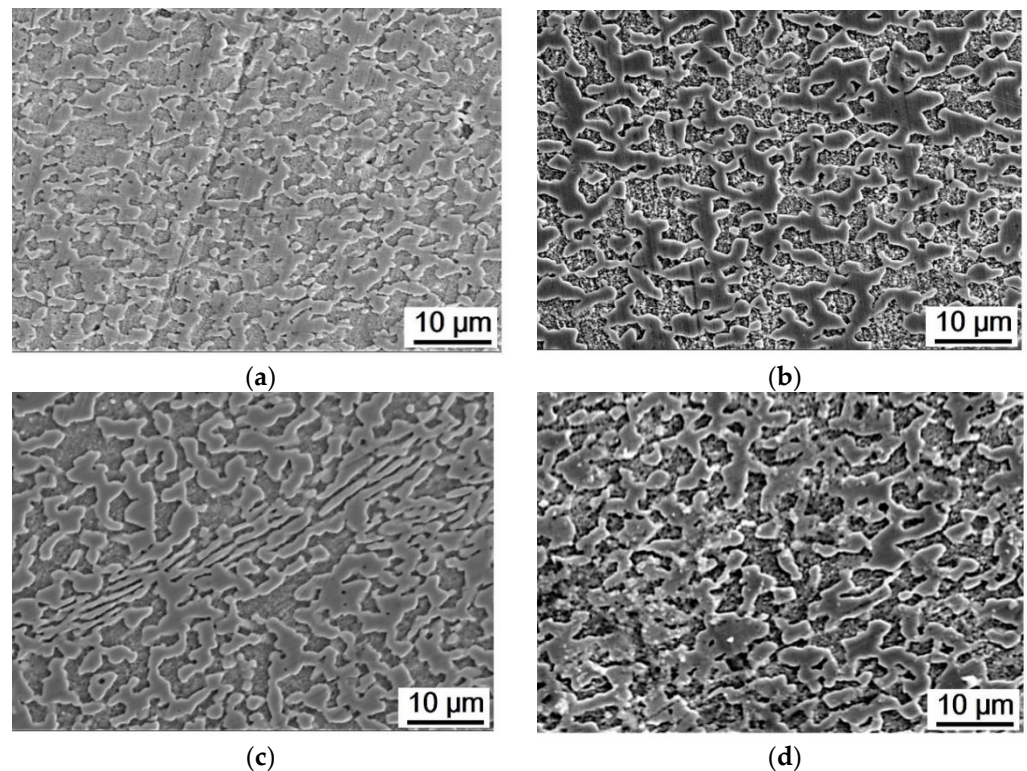


Figure 5. Microstructures of the Bi–Sn samples after t-HPS processing for five turns and storage at RT for (a) 8 h, (b) 2 days, (c) 7 days and (d) 21 days.

FIB was employed to mill the samples and observe these Sn particles within the Bi phase. The solubility of the second phase was higher in the melted state compared to the

solid state, therefore these Sn second-phase particles may participate in solidification and become trapped within the Bi phase. As the material is subjected to t-HPS processing, tips of the large Sn phase may be broken and mixed into the Bi phase through the flow of the materials under shear deformation. This is shown in Figure 6b where the number of visible Sn particles inside the Bi phase is larger compared to Figure 6a. Unfortunately, it was not feasible to compare the mean size of these particles as the number of visible particles was not sufficient. It is also observed that the grain boundaries inside each phase were visible after fine milling.

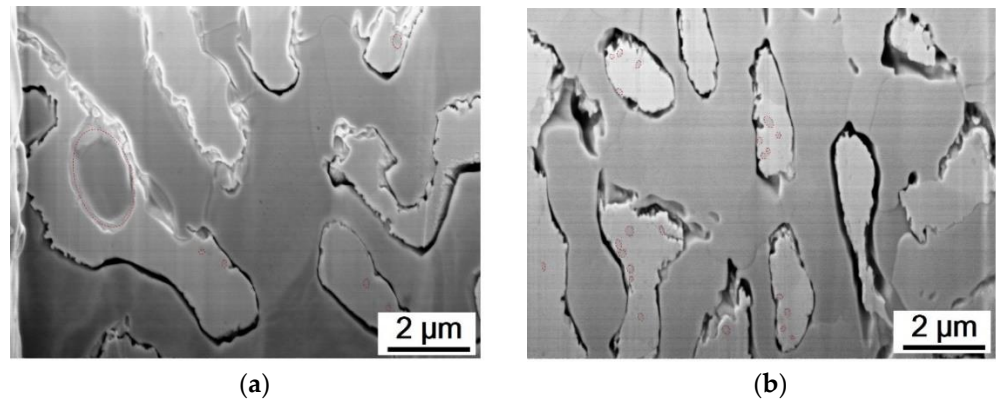


Figure 6. Microstructures (a) of the as-cast Bi–Sn sample and (b) after t-HPS processing for five turns and storage at RT for 8 h.

Tensile tests were conducted on the Bi–Sn samples and the main results of each sample under various initial strain rates are shown in Table 1. The results demonstrate that the superplasticity of the Bi–Sn alloy was significantly improved by t-HPS processing and elongations to failure of more than 1500% and 1800% were achieved in the sample processed by t-HPS for 5 and 20 turns, respectively. For all the samples, smaller strain rates were favorable for having higher elongations to failure.

Table 1. Tensile properties of the Bi–Sn samples under various initial strain rates at RT.

Strain Rate	$1.0 \times 10^{-2} \text{ s}^{-1}$		$1.0 \times 10^{-3} \text{ s}^{-1}$		$1.0 \times 10^{-4} \text{ s}^{-1}$	
	UTS, MPa	Elongation	UTS, MPa	Elongation	UTS, MPa	Elongation
As-cast	70	~40%	60	~80%	53	~130%
0.25 turns	69	~80%	48	~280%	33	~430%
1 turn	69	~100%	49	~270%	31	~490%
5 turns	/	/	42	~1170%	23	~1530%
20 turns	/	/	26	~1060%	12	~1820%

In this study, an elongation of >1800% was achieved in the Bi–Sn (57/43) sample after t-HPS processing for 20 turns. In an earlier study, a Bi–Sn (58/42) sample processed by HPT for 10 turns featured a superplastic elongation of around 1220% under a strain rate of $1 \times 10^{-4} \text{ s}^{-1}$ at RT. Thus, the tensile samples of this study were generally more superplastic and exhibited larger elongations to failure than those processed by HPT [16]. Nevertheless, it should be noted that an elongation of 1900% was achieved in a very early study using larger rod samples of the same alloy after extrusion [18].

4. Discussion

During t-HPS processing, the imposed shear strains are around 16.5, 66, 330 and 1300 for 0.25, 1, 5 and 20 turns of processing, respectively [13]. The tube sample used in this investigation had a large diameter of around 47 mm and the wall thickness of the tube

sample was around 2.7 mm. It is reasonable to expect that during t-HPS processing the tube sample deformed very close to simple shear. By contrast, during HPT processing, the sample is in the form of a thin disk which normally has a diameter of 10 mm and thickness of around 0.8 mm so that the deformation along the radius of the disk is inhomogeneously distributed. This geometry and the overall inhomogeneous nature would lead to a significant disorder in the manner of deformation since the material located at a larger radial position on the disk must drag the material which is located closer to the center. Such a combined deformation of shear and rotation during HPT is more efficient in refining the microstructure of materials. Thus, during t-HPS processing of the Bi–Sn alloy, the original lamellar structure is randomly packed together. These lamellae lie perpendicular to the shear direction and tend to fracture first to accumulate the shear strain [23,24]. Moreover, the Bi–Sn alloy exhibits a significant strain-induced softening behavior and this behavior leads to a lower hardness value within the shear-localized zones which may in turn aggravate the shear inhomogeneity. As shown in Figure 3, the preserved lamellar bands are mostly parallel to each other. It is apparent that the Bi–Sn sample processed by t-HPS for 20 turns had not yet reached a saturated state as shown in Figure 3b, although the imposed shear strain was as large as 1300. More strain is therefore needed until all of these preserved lamellar structures disappear.

As shown in the SEM images, lamellar structures of the Bi phase and the Sn phase were mutually contained within each other, as shown in Figure 1a. Such a lamella-dominating structure exists after t-HPS for low numbers of turns as shown in Figure 1b,c. The absolute melting temperature, T_m , of the Bi–Sn eutectic alloy is around 412 K and therefore the ambient room temperature is around $0.7 T_m$ for the alloy [25–29]. It is widely recognized that the ductility of materials in tensile testing at elevated temperatures is related to the dislocation movement and/or grain boundary sliding behavior [30]. For this alloy, it is rather difficult for dislocations to pass through the interfaces at phase boundaries. Moreover, boundary sliding at the phase boundaries is also very difficult in the as-cast Bi–Sn alloy as the Bi phase and the Sn phase lamellar structures are closely interlocked within each other [31–34]. It is reasonable to expect, therefore, that the ductility of the as-cast Bi–Sn alloy will be poor due to its lamellar structure, and this is confirmed in these experiments where the as-cast alloy had an elongation of only around 130% under a strain rate of $1.0 \times 10^{-4} \text{ s}^{-1}$. Nevertheless, after t-HPS processing for large numbers of turns, the two phases experience diastrophism under the action of a large shear force. This large shear force gradually destroys the lamellar locking between the two phases and large numbers of grain boundaries are formed inside each phase. In practice, these new grain boundaries probably act as favorable sites for grain boundary sliding so that, as a result, the ductility of the Bi–Sn sample becomes significantly improved after t-HPS processing for large numbers of turns. In this study, the recorded elongations of >1000% easily fulfilled the requirement of an elongation of >400% in order to achieve true superplastic flow [35].

Grain growth and phase growth also occur in the Bi–Sn alloy during storage, giving the self-annealing effect. At the same time, the second-phase particles continuously precipitate out from the matrix. These grain growth and phase growth are the dominating factors controlling the increasing hardness during storage at RT.

5. Summary and Conclusions

1. Experiments on a Bi–Sn (57/43) eutectic alloy showed that t-HPS processing gradually refined the microstructure and led to decreasing microhardness.
2. Shear localization of the eutectic structure during t-HPS processing was observed, but some preserved dense lamellar bands were visible even after t-HPS processing for 20 turns.
3. The Bi–Sn (57/43) alloy processed by t-HPS showed significantly enhanced superplasticity, with elongations up to >1000%. This is attributed to the breaking of the lamellar structure and the presence of a refined grain size.

Author Contributions: Methodology, Y.H., J.-T.W. and T.G.L.; validation, C.-T.W. and Z.L.; investigation, C.-T.W.; resources, Y.H., J.-T.W. and T.G.L.; data curation, C.-T.W. and Z.L.; writing—original draft preparation, C.-T.W.; writing—review and editing, Y.H., J.-T.W. and T.G.L.; supervision, T.G.L.; project administration, T.G.L.; funding acquisition, Y.H., J.-T.W. and T.G.L. All authors have read and agreed to the published version of the manuscript.

Funding: This work was supported by the National Science Foundation of the United States (grant No. DMR-1160966), the European Research Council (ERC Grant Agreement No. 267464-SPDMETALS) and the Natural Science Foundation of China (grant No. 52074160).

Data Availability Statement: The raw and processed data generated during this study will be made available upon reasonable request.

Acknowledgments: The authors thank L.Y. Li and Y. Yang of NJUST for assistance with t-HPS processing.

Conflicts of Interest: The authors declare no conflict of interest.

References

1. Valiev, R.Z.; Estrin, Y.; Horita, Z.; Langdon, T.G.; Zehetbauer, M.J.; Zhu, Y.T. Producing bulk ultrafine-grained materials by severe plastic deformation. *JOM* **2006**, *58*, 33–39. [[CrossRef](#)]
2. Barnes, A.J. Superplastic forming 40 years and still growing. *J. Mater. Eng. Perform.* **2007**, *16*, 440–454. [[CrossRef](#)]
3. Langdon, T.G. Twenty-five years of ultrafine-grained materials: Achieving exceptional properties through grain refinement. *Acta Mater.* **2013**, *61*, 7035–7059. [[CrossRef](#)]
4. Valiev, R.Z.; Langdon, T.G. Principles of equal-channel angular pressing as a processing tool for grain refinement. *Prog. Mater. Sci.* **2006**, *51*, 881–981. [[CrossRef](#)]
5. Zhilyaev, A.P.; Langdon, T.G. Using high-pressure torsion for metal processing: Fundamentals and applications. *Prog. Mater. Sci.* **2008**, *53*, 893–979. [[CrossRef](#)]
6. Zhilyaev, A.P.; Kim, B.K.; Nurislamova, G.V.; Baró, M.D.; Szpunar, J.A.; Langdon, T.G. Orientation imaging microscopy of ultrafine-grained nickel. *Scripta Mater.* **2002**, *46*, 575–580. [[CrossRef](#)]
7. Zhilyaev, A.P.; Nurislamova, G.V.; Kim, B.K.; Baró, M.D.; Szpunar, J.A.; Langdon, T.G. Experimental parameters influencing grain refinement and microstructural evolution during high-pressure torsion. *Acta Mater.* **2003**, *51*, 753–765. [[CrossRef](#)]
8. Wongsan-Ngam, J.; Kawasaki, M.; Langdon, T.G. A comparison of microstructures and mechanical properties in a Cu-Zr alloy processed using different SPD techniques. *J. Mater. Sci.* **2013**, *48*, 4653–4660. [[CrossRef](#)]
9. Brodova, I.; Rasposienko, D.; Shirinkina, I.; Petrova, A.; Akopyan, T.; Bobruk, E. Effect of severe plastic deformation on structure refinement and mechanical properties of the Al-Zn-Mg-Fe-Ni Alloy. *Metals* **2021**, *11*, 296. [[CrossRef](#)]
10. Edalati, K.; Li, H.-W.; Kilmametov, A.; Floriano, R.; Borchers, C. High-Pressure Torsion for Synthesis of High-Entropy Alloys. *Metals* **2021**, *11*, 1263. [[CrossRef](#)]
11. Nocivin, A.; Raducanu, D.; Vasile, B.; Trisca-Rusu, C.; Cojocaru, E.; Dan, A.; Irimescu, R.; Cojocaru, V. Tailoring a Low Young Modulus for a Beta Titanium Alloy by Combining Severe Plastic Deformation with Solution Treatment. *Materials* **2021**, *14*, 3467. [[CrossRef](#)]
12. Svirid, A.; Pushin, V.; Kuranova, N.; Makarov, V.; Ustyugov, Y. Structural and Phase Transformations and Physical and Mechanical Properties of Cu-Al-Ni Shape Memory Alloys Subjected to Severe Plastic Deformation and Annealing. *Materials* **2021**, *14*, 4394. [[CrossRef](#)]
13. Wang, J.T.; Li, Z.; Wang, J.; Langdon, T.G. Principles of severe plastic deformation using tube high-pressure shearing. *Scr. Mater.* **2012**, *67*, 810–813. [[CrossRef](#)]
14. Li, Z.; Zhang, P.F.; Yuan, H.; Lin, K.; Liu, Y.; Yin, D.L.; Wang, J.T.; Langdon, T.G. Principle of one-step synthesis for multilayered structures using tube high-pressure shearing. *Mater. Sci. Eng. A* **2016**, *658*, 367–375. [[CrossRef](#)]
15. Meng, J.J.; Li, Z.; Liu, Y.; Bin Zhu, Y.; Wang, S.; Lin, K.; Tao, J.Q.; Wang, J.T. Investigation on the Strain Distribution in Tube High-Pressure Shearing. *Metals* **2019**, *9*, 1117. [[CrossRef](#)]
16. Wang, C.T.; He, Y.; Langdon, T.G. The significance of strain weakening and self-annealing in a superplastic Bi-Sn eutectic alloy processed by high-pressure torsion. *Acta Mater.* **2019**, *185*, 245–256. [[CrossRef](#)]
17. Wang, C.T.; Langdon, T.G. An examination of strain weakening and self-annealing in a Bi-Sn alloy processed by high-pressure torsion. *Mater. Lett.* **2021**, *301*, 130321. [[CrossRef](#)]
18. Pearson, C.E. The viscous properties of extruded eutectic alloys of lead-tin and bismuth-tin. *J. Inst. Met.* **1934**, *54*, 111–124.
19. Kawasaki, M.; Ahn, B.; Langdon, T.G. Microstructural evolution in a two-phase alloy processed by high-pressure torsion. *Acta Mater.* **2009**, *58*, 919–930. [[CrossRef](#)]
20. Zhang, N.X.; Kawasaki, M.; Huang, Y.; Langdon, T.G. Microstructural evolution in two-phase alloys processed by high-pressure torsion. *J. Mater. Sci.* **2012**, *48*, 4582–4591. [[CrossRef](#)]
21. Zhang, N.X.; Chinh, N.Q.; Kawasaki, M.; Huang, Y.; Langdon, T.G. Self-annealing in a two-phase Pb-Sn alloy after processing by high-pressure torsion. *Mater. Sci. Eng. A* **2016**, *666*, 350–359. [[CrossRef](#)]

22. Zhang, N.X.; Kawasaki, M.; Huang, Y.; Langdon, T.G. An examination of microstructural evolution in a Pb–Sn eutectic alloy processed by high-pressure torsion and subsequent self-annealing. *Mater. Sci. Eng. A* **2020**, *802*, 140653. [[CrossRef](#)]
23. Wang, J.; Kang, S.-B.; Kim, H. Microstructure transformation from lamellar to equiaxed microduplex through equal-channel angular pressing in an Al-33 pct Cu eutectic alloy. *Met. Mater. Trans. A* **2004**, *35*, 279–286. [[CrossRef](#)]
24. Wang, J.; Kang, S.-B.; Kim, H. Shear features during equal channel angular pressing of a lamellae eutectic alloy. *Mater. Sci. Eng. A* **2004**, *383*, 356–361. [[CrossRef](#)]
25. Massalski, T.B. *Binary Alloy. Phase Diagrams*, 2nd ed.; ASM International: Materials Park, OH, USA, 1990; pp. 794–796.
26. Ren, G.; Collins, M.N. Improved Reliability and Mechanical Performance of Ag Microalloyed Sn58Bi Solder Alloys. *Metals* **2019**, *9*, 462. [[CrossRef](#)]
27. Wang, K.; Wang, F.; Huang, Y.; Qi, K. Comprehensive Properties of a Novel Quaternary Sn-Bi-Sb-Ag Solder: Wettability, Interfacial Structure and Mechanical Properties. *Metals* **2019**, *9*, 791. [[CrossRef](#)]
28. Liu, Y.; Tu, K.N. Low melting point solders based on Sn, Bi, and In elements. *Mater. Today Adv.* **2020**, *8*, 100115. [[CrossRef](#)]
29. Kang, H.; Rajendran, S.H.; Jung, J.P. Low melting temperature Sn-Bi solder: Effect of alloying and nanoparticle addition on the microstructural, thermal, interfacial bonding, and mechanical characteristics. *Metals* **2021**, *11*, 364. [[CrossRef](#)]
30. Langdon, T.G. A unified approach to grain boundary sliding in creep and superplasticity. *Acta Metall. Mater.* **1994**, *42*, 2437–2443. [[CrossRef](#)]
31. Hu, X.; Li, K.; Ai, F. Research on lamellar structure and micro-hardness of directionally solidified Sn-58Bi eutectic alloy. *China Foundry* **2012**, *9*, 360–365.
32. Lee, H.B.; Kim, Y.W.; Kim, S.H.; Park, S.H.; Choi, J.-P.; Aranas, C., Jr. A Modular Solder System with Hierarchical Morphology and Backward Compatibility. *Small* **2018**, *14*, e1801349. [[CrossRef](#)]
33. Kim, S.H.; Yeon, S.-M.; Kim, J.H.; Park, S.J.; Lee, J.E.; Park, S.-H.; Choi, J.-P.; Aranas, C.J.; Son, Y. Fine Microstructured In–Sn–Bi Solder for Adhesion on a Flexible PET Substrate: Its Effect on Superplasticity and Toughness. *ACS Appl. Mater. Interfaces* **2019**, *11*, 17090–17099. [[CrossRef](#)] [[PubMed](#)]
34. Xu, K.-K.; Zhang, L.; Gao, L.-L.; Jiang, N.; Zhang, L.; Zhong, S.-J. Review of microstructure and properties of low temperature lead-free solder in electronic packaging. *Sci. Technol. Adv. Mater.* **2020**, *21*, 689–711. [[CrossRef](#)] [[PubMed](#)]
35. Langdon, T.G. Seventy-five years of superplasticity: Historic developments and new opportunities. *J. Mater. Sci.* **2009**, *44*, 5998–6010. [[CrossRef](#)]